RSC Sustainability

ROYAL SOCIETY OF CHEMISTRY

PAPER

View Article Online
View Journal | View Issue

Cite this: *RSC Sustainability*, 2024, **2**, 2709

Excellent phosphorus-doped porous carbon oxygen reduction reaction catalysts derived from natural wild *Angelica dahurica*

Wenhao Mo,* Xiaohua Tan and Lei Zhao

Received 18th April 2024
Accepted 22nd July 2024

DOI: 10.1039/d4su00182f

rsc.li/rscsus

At present, phosphorus-doped porous carbon–oxygen reduction catalysts prepared by chemical methods are not able to achieve good performance. In order to improve the catalytic performance of the phosphorus-doped oxygen reduction reaction (ORR), wild *Angelica dahurica* (WAD) with abundant phosphorus was used as a carbon carrier and phosphorus source at the same time. Phosphorus-doped carbon-based materials based on carbonization of biomaterials also had a homogeneous structure and excellent stability. WAD directly carbonized at 900 °C (WAD-900) had a half-wave potential of 0.822 V relative to a reversible hydrogen electrode, a limiting current density of 4.54 mA cm^{-2} at 1600 rpm, an average number of transferred electrons of four, and a stability of 95.9% for 20 000 s, larger than the 82.6% of Pt/C. This study demonstrates the excellent performance of naturally occurring phosphorus dopants in oxygen reduction reactions and their favorable catalysis properties, opening up a new direction for chemical dopants that find it difficult to achieve good performance.

Sustainability spotlight

In order to improve the reduction catalyst performance of the phosphorus-doped oxygen reduction reaction (ORR), catalysts were obtained by high-temperature calcination of wild *Angelica dahurica*, which is rich in phosphorus. Reduction catalysts prepared with wild *Angelica dahurica* have many advantages. As a plant, wild *Angelica dahurica* is a renewable resource. The reduction catalyst in this paper is a carbon-based organic material naturally doped with a variety of trace elements, and it does not contain heavy metals that pollute the environment. After being made into a battery, even after being discarded, it can be decomposed naturally and does not cause harm to the environment. The use of this raw material as a battery oxygen reduction catalyst can not only reduce CO_2 emissions, but also reduce heavy metal pollution of the environment.

1. Introduction

Atomic-doped carbon materials are widely used as cathode catalysts; in particular, nitrogen-doped carbon catalysts are often researched. On the basis of nitrogen doping, iron nitrogen carbon has made long-term progress.[1–3] Compared to that, doping with phosphorus, in the same group as nitrogen, shows lower performance, and there is less phosphorus-based ternary doping. In contrast to the N atom, the P atom has lower electronegativity and larger atomic size, the 3P orbital has lone-pair electrons, and the doping entry site better regulates the lone-pair electrons of O_2 and is more conducive to the adsorption and reduction of O_2,[4,5] which give P-doped carbon better catalytic performance. However, at present, phosphorus–carbon catalysts show lower performance than nitrogen-doped porous carbon catalysts. The reason is that C–P is difficult to obtain. Now, the main task is how to improve the electrocatalytic properties of phosphorus-doped porous carbon to obtain a better P-doped oxygen reduction reaction (ORR) or provide a foundation for a ternary composite of metal, phosphorus and carbon.

Table 1 shows the content of phosphorus doping and the performance of ORR. Contrasting the content of P-doping, the results show that the best content of P-doping in the better catalysts is not more than 3%. Because the chemical method does not achieve a better ORR result, is extremely vital to decide how to obtain a rational method of P-doping.

As we all know, many natural plants have a P content larger than 3%. In order to improve the performance of phosphorus-doped porous carbon catalysts, we chose the WAD plant with a high P content as the carbon-based material for catalyst preparation. The pore structure of WAD with biological materials can provide natural channels and reaction sites for porous carbon doping. At the same time, biological materials after carbonization not only show a homogeneous and stable structure but also achieve a rational phosphorus content and structure by carbonization.

In this paper, we directly carbonize the WAD biomaterial, based on the poor doping effect of chemically reacted

School of Physical Science and Technology, Lingnan Normal University, Zhanjiang, 524048, China. E-mail: mowenhaobiaodi@126.com

Table 1 The phosphorus content and ORR index of phosphorus-doped carbon materials tested in 0.1 M KOH saturated with O_2

Material	Doping method	Content of P-doped	ORR activity *vs.* Pt/C	Reference
Phosphorus-doped hollow d carbon	Tetraphenylphospho-niumbromide	1.61 at%	52 mV lower than Pt/C (half-wave potential)	6
P-doped carbon xerogel	H_3PO_4	1.64 at%	70 mV of initial lower than Pt/C (half-wave potential)	7
Phosphorus-doped graphene	TPP	1.81 at%	30 mV lower than Pt/C (onset potential)	8
Phosphorus-doped carbon nanosheets	P_2O_5	1.75 at%	40 mV lower than Pt/C (onset potential)	9
Phosphorus-doped graphene nanosheets	$BminPF_6$	1.16 at%	23.5 mV lower than Pt/C (onset potential)	10
N-and P-doped biocarbon	Yeast	2.62 at%	29 mV lower than Pt/C (half-wave potential)	11
Phosphorus and iron doped nitrogen-containing carbon	Shrimp shell	1.42 at%	20 mV lower than Pt/C (half-wave potential)	12

phosphorus. Phosphorus is distributed in different structures during plant growth, so this naturally introduces phosphorus and improves the diversity of phosphorus-doped carbon, producing phosphorus-doped carbon catalysts with stable homogeneous structures and different phosphorus groups. Through the study of WAD, it is found that it shows excellent phosphorus-doped ORR performance. The maximum amount of P in WAD carbon-based materials is 1.82 at%. The phosphorus content of the WAD-900 catalyst is within the standard of 1.45 at% and it has a high total proportion of P–C. The limiting current density tested in a 0.1 M KOH solution saturated with O_2 is 4.54 mA cm^{-2}. At 1600 rpm, the average number of transferred electrons is close to four. The stability is 95.9% after 20 000 s of testing at a speed of 1600 rpm, which is larger than the 82.6% of a Pt/C catalyst. It is hoped that this study will provide a new idea for research into phosphorus-doped carbon materials and iron–phosphorus–carbon composites for which it is difficult to obtain good properties by chemical methods.

2. Experimental

2.1 Sample preparation

Before heat treatment, the WAD biomass was dried at 100 °C for 12 h. The dried WAD was placed in a tube furnace and heated at 400 °C for 1 h. Next, the obtained carbon material was directly carbonized at 800 °C, 900 °C, and 1000 °C for 1 h at a heating rate of 10 °C min^{-1} at a flow rate of 100 mL min^{-1} in an N_2 atmosphere. After carbonization, the sample was washed several times with distilled water and dried at 60 °C. WAD carbonized at 800 °C, 900 °C, and 1000 °C are labelled WAD-800, WAD-900, and WAD-1000, respectively.

2.2 Preparation of the working electrodes

GC electrodes needed to be prepared prior to measurement. The GC electrodes were polished with gamma alumina powders (0.05 mm) until a bright mirror surface was obtained; then washed with distilled water and ethanol and dried in a vacuum. Then, an appropriate amount of catalyst was placed on the surface of the GC electrode to achieve a content of 600 μg cm^{-2}. Finally, a drop of Nafion solution (5 wt%, Dupont) was dropped on the catalyst layer to improve adhesion to the GC surface. After drying naturally at room temperature, it was tested. To eliminate the influence of the background current, CV and RDE curves were tested in O_2 or N_2 saturated 0.1 M KOH solutions.

2.3 Characterization of samples

The morphology and structure of the samples were separately checked by a scanning electron microscope (SEM), transmission electron microscope (TEM), X-ray diffraction (XRD), and X-ray photoelectron energy spectroscopy (XPS). A electrochemical workstation (RST5200F) was used to measure cyclic voltammetry (CV) and a rotating disk device from Shanghai Goldsmiths was used to measure the RDE polarization curve. A carbon rod electrode and an Ag/AgCl (sat.) (CHI111) electrode were used as the counter electrode and reference electrode. The working electrode uses a glassy carbon (GC) electrode (diameter 4 mm, 0.1256 cm^2, CHI104). The Ag/AgCl (sat.) (CHI111) electrode is converted into a reversible hydrogen electrode (RHE) by applying 1.01 V.

3. Results and discussion

Fig. 1(a) shows images of WAD. As shown in Fig. 1, the structure of WAD-800, WAD-900 and WAD-1000 carbon materials is a layered structure. As the temperature increases, the diameter and wall thickness gradually decrease, the wall thickness of the hole is reduced from about 1 μm to about 500 nm, and more folds and particles appear on the surface of the layered structure, with visible pores, and a spacious mass transfer channel, conducive to mass transport at the active site.[13]

Fig. 2 shows a mapping of WAD-900, which includes the main elements of C, P, O, and N, and a small amount of Fe, Ca, and K. In fact, when measuring the atomic content percentage of each element in the mapping, the atomic content percentage of Fe is 0. This is possible because the content of Fe is too low to be detected. The cross-section of the WAD-900 material is a random folded structure arranged in a sheet-like shape, which can form a smooth transmission channel inside the WAD material to accelerate the transfer and transmission of electrons. Meanwhile, these pore structures produce various defects, and these defects have been shown to favor the performance of ORR.[13]

Fig. 3a shows the low magnification transmission image of WAD-900, while Fig. 3b and c show the high-magnification

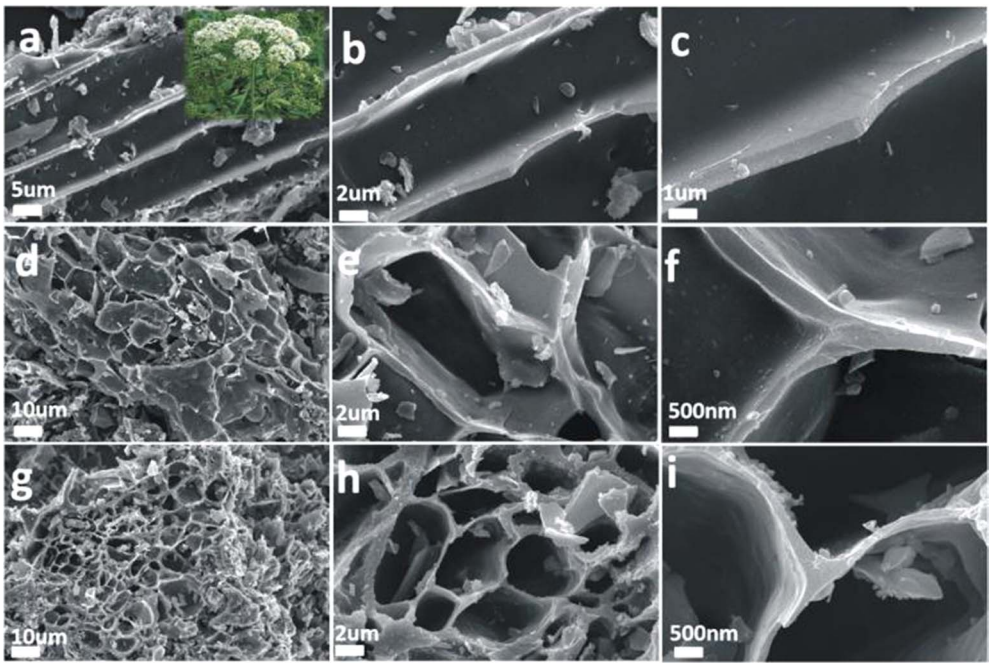

Fig. 1 WAD-800 SEM images (a–c), scale bars are 5 μm, 2 μm, and 1 μm; WAD-900 SEM images (d–f) and WAD-1000 SEM images (g–i), the scale bars are 10 μm, 2 μm, and 500 nm, respectively.

transmission images, with a spacing of approximately 0.34 nm corresponding to the (200) crystal plane of graphitic carbon. The temperature of the surface carbonization zone increases with the increase in temperature. The elemental mapping (obtained from Fig. 3a) shows that C, O, N, and P are well dispersed, with P being more pronounced and having an elemental content an order of magnitude higher than that of N. From the mapping diagram (Fig. 3d), it can be proved that the distribution of phosphorus is relatively uniform, which is directly related to the natural phosphorus doping of the WAD plant.

Fig. 4a shows the XRD spectra at different carbonization temperatures. Two characteristic diffraction peaks can be observed from the figure, indicating that all the materials have

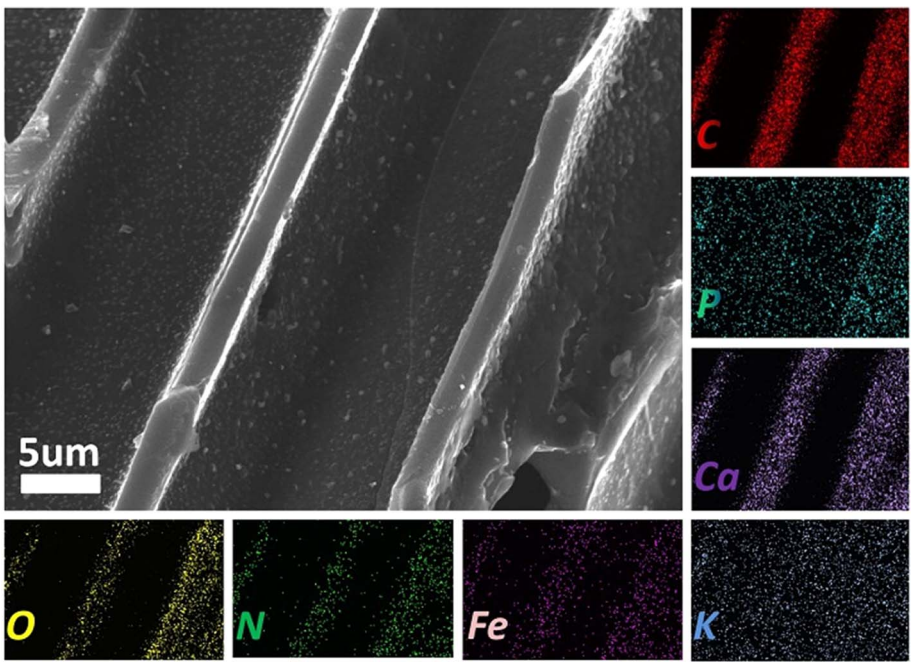

Fig. 2 Elemental mapping images of WAD-900 and corresponding energy spectrum element diagram with a scale of 5 μm.

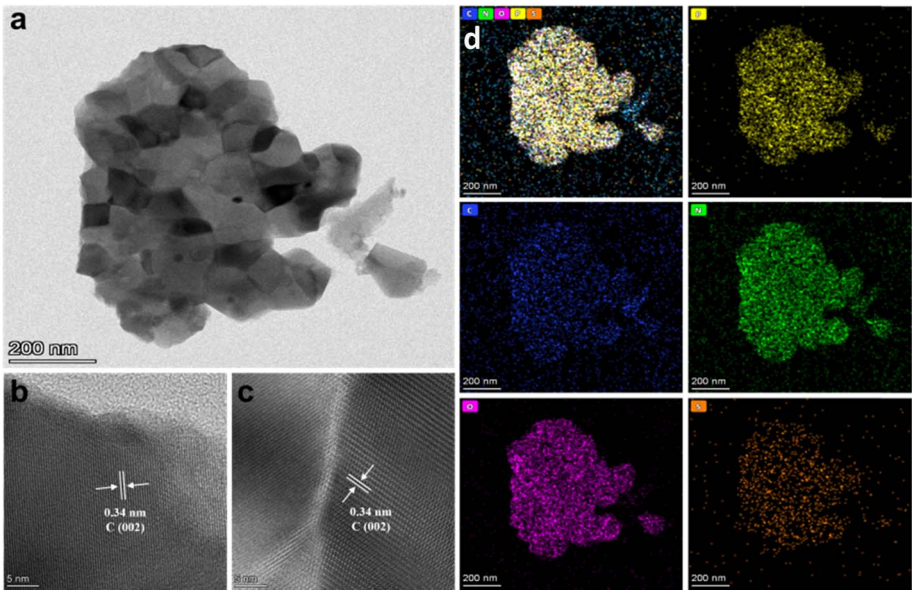

Fig. 3 (a) WAD-900 TEM, (b and c) the FFT filtered TEM images of different selected regions, and (d) the corresponding elemental mapping analysis of WAD-900.

an amorphous structure.[14] With an increase in carbonization temperature, the (002) diffraction peak broadens and the intensity becomes weaker, indicating that the graphitized structure of the material continues to decrease. The intensity of the diffraction peak is weakest when the carbonization temperature is 900 °C. The structure of the phosphorus-doped porous carbon materials is more disordered and exhibits more defects, which is conducive to increasing the catalytic sites. There is no metal residual peak in the figure, and it may be that the Fe content is too low to detect.

The Raman spectra of WAD at 800 °C, 900 °C and 1000 °C are shown in Fig. 4b. Raman spectra of all the samples exhibited two characteristic peaks located at around 1345 cm^{-1} (D band) and 1590 cm^{-1} (G band). The intensity ratios, I_D/I_G, of the D band and G band of the samples at 800 °C, 900 °C and 1000 °C are: 1.053 for WAD-800, 1.048 for WAD-900, and 1.027 for WAD-1000. The I_D/I_G ratio decreases with increasing carbonization temperature, indicating that the carbonization temperature affects the structure of carbon materials. Compared with WAD-1000, the I_D/I_G of WAD-800 and WAD-900 have a high value in the Raman spectrum, indicating that the structure is more disordered and there are more defects on the surface, which can form catalytic sites[15] and improve conductivity and charge transfer.[9] In order to further analyze the reasons for disorder, we conducted XPS to compare and analyze the changes in phosphorus doping content at different temperatures and the effects of carbon phosphorus bonds on carbon disorder.

The XPS spectrum of WAD shown in Fig. 5a, which includes a C1s peak (~284.5 eV), an O1s peak (~532.0 eV), an N1s peak (~400.0 eV), a P2p peak (~133.3 eV), and an Fe2p peak (~725.0 eV), confirms the successful doping of Fe, N and P.[16–19] The high-resolution XPS spectra of N1s for WAD-800 (Fig. 6a), WAD-

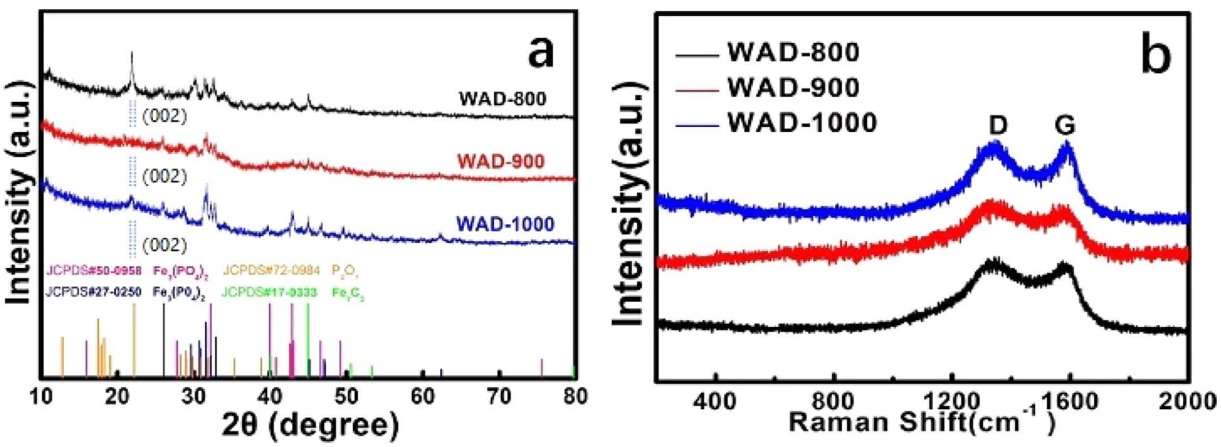

Fig. 4 (a) XRD patterns of WAD-800, WAD-900 and WAD-1000, (b) Raman spectra of WAD-800, WAD-900 and WAD-1000.

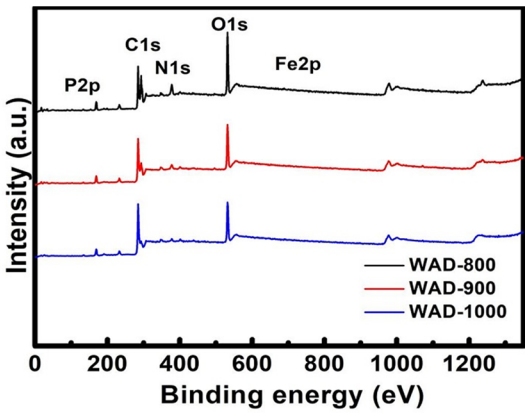

Fig. 5 Total XPS spectra.

900 (Fig. 6b) and WAD-1000 (Fig. 6c), can be divided into five peaks: pyridinic-N (398.7 ± 0.3 eV), Fe–N (399.6 ± 0.2 eV), pyrrolic-N (400.3 ± 0.3 eV), quaternary-N (401.4 ± 0.5 eV), and pyridine-N-O (402–405 eV).[15] A large number of studies have shown that pyridinic-N is conducive to electron transfer to enhance catalytic activity.[20] With increasing temperature, the total content of pyridinic-N (green) and quaternary-N (dark yellow) of WAD-900 is 47.8%, greater than 44.5% of WAD-800 and 45.3% of WAD-1000, and provides more active sites in ORR.[15]

The high-resolution XPS spectra of P2p for WAD-800 (Fig. 6d), WAD-900 (Fig. 6e) and WAD-1000 (Fig. 6f) can be divided into two peaks: P–O (133.6 eV), P–C (132.2 eV).[21,22] The content of P–O is higher than that of P–C at different temperatures, which proves that P–O is the main doping type of P. This is due to the higher electronegativity of O (3.44), which can

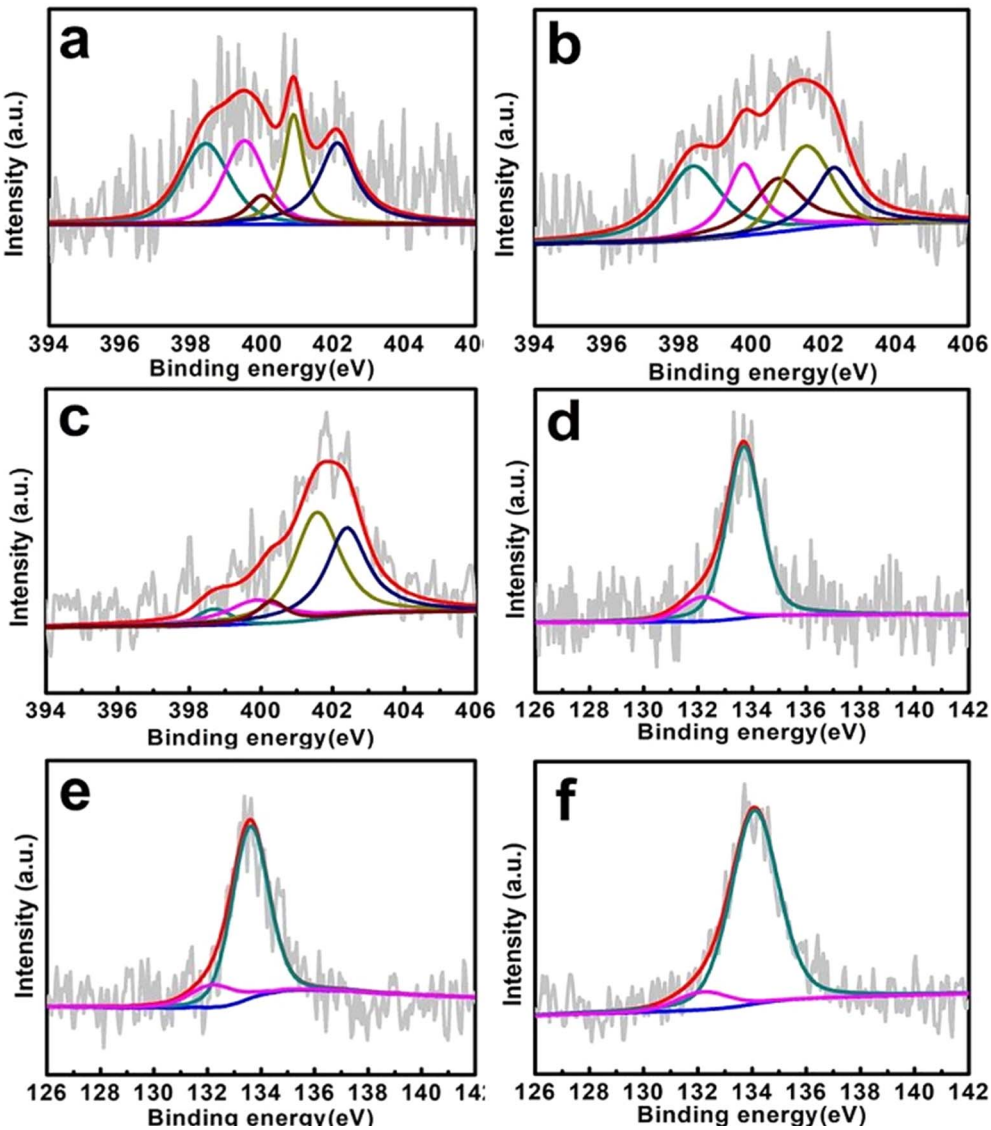

Fig. 6 (a–c) represent the N1s spectra of WAD-800, WAD-900, WAD-1000 (dark cyan: pyridinic-N, magenta: Fe–N, wine: pyrrolic-N, dark yellow: pyrrolic-N, navy: pyridine-N-O); (d–f) represent the P2p spectra of WAD-800, WAD-900, and WAD-1000 respectively (magenta: P–C, dark cyan: P–O).

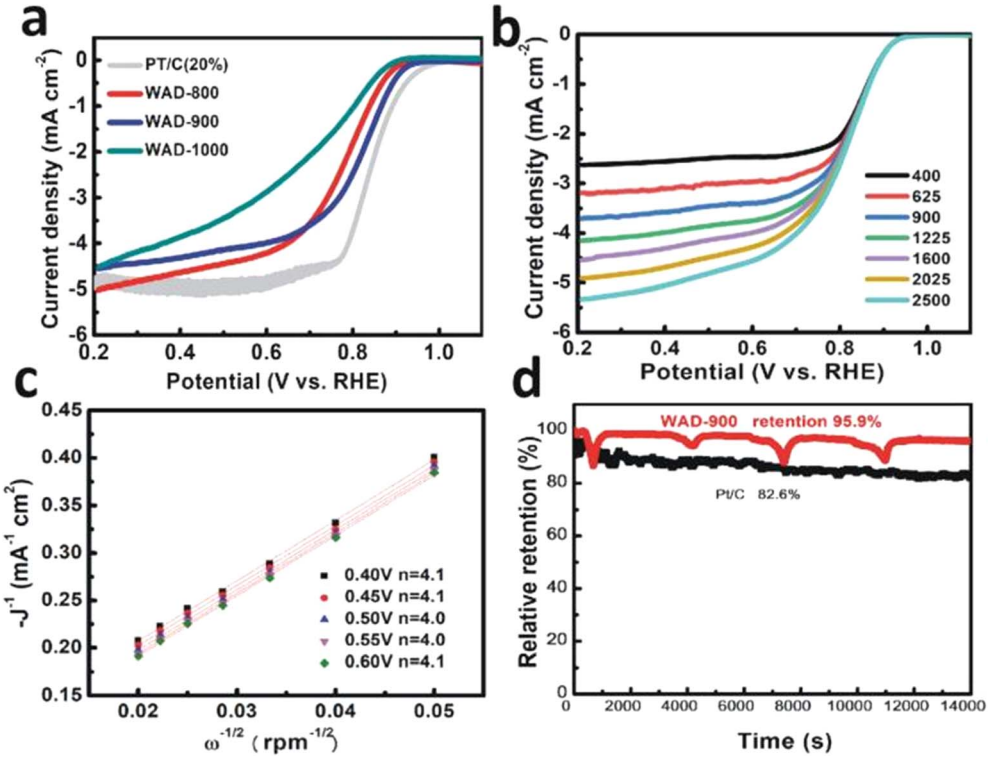

Fig. 7 (a) Linear sweep voltammograms of WAD-800, WAD-900, WAD-1000, and Pt/C catalysts in O_2-saturated 0.1 M KOH solution with testing conditions of 1600 rpm min^{-1} and 10 mV s^{-1}. (b) Polarization curves for ORR in an O_2-saturated 0.1 M KOH solution on WAD-900 electrodes with rotation rates from 400 to 2500 rpm. (c) Koutecky–Levich plots of the WAD-900 electrode at different potentials and their corresponding electron transfer number. (d) Current–time chronoamperometric response for WAD-900 and Pt/C (20%) catalysts tested at 0.6 V (*vs.* RHE) at a rotation speed of 1600 rpm.

enhance the electron barrenness in C atoms.[23] The content of P–C (purple) in WAD-900 is 15.0%, greater than the 14.29% of WAD-800 and 8.65% of WAD-1000. These two structures (P–O and P–C) have been reported to be beneficial to ORR.[23–26] P doping can induce negative delocalization of C atoms adjacent to P atoms. At the same time, the oxygen atoms in the P–O bond can increase the electron poverty of carbon atoms and increase electron delocalization.[26]

By comparing the obtained RDE curves of different catalysts (Fig. 7a), it can be observed that WAD-900 exhibits better ORR activity, with an initial potential of 0.965 V, a half-wave potential of 0.822 V, which is 30 mV lower than the half-peak potential of commercial Pt/C (20%), with a limiting current density of 4.54 mA cm^{-2}. The LSV curve of WAD-900 (Fig. 7b) shows that at a constant starting potential, the current density is determined by the speed,[27] through the Koutecky–Levich (K–L) equation[8]

$$\frac{1}{J} = \frac{1}{J_L} + \frac{1}{J_K} = \frac{1}{B\omega^{\frac{1}{2}}} + \frac{1}{J_K} \quad (1)$$

$$B = 0.2nFC_0D_0^{\frac{2}{3}}V^{-\frac{1}{6}} \quad (2)$$

where J, J_K and J_L are the measured current density, kinetic limiting current density and diffusion limiting current density, respectively; ω is angular velocity; n and F are the electron transfer number and Faraday constant ($F = 96\,485$ C mol^{-1}); C_0 and D_0 are the volumetric concentration of O_2 ($C_0 = 1.2 \times 10^{-6}$ mol cm^{-3}) and the diffusion coefficient of O_2 ($D_0 = 1.9 \times 10^{-5}$ cm^2 s^{-1}); and V is the kinetic viscosity of the electrolyte ($V = 0.01$ cm^2 s^{-1}). As a result, the average number of transferred electrons is close to four from 0.4 to 0.6 V (Fig. 7c). Besides, these strings are linear and parallel, indicating that the ORR process of WAD-900 follows first-order kinetics in the selected potential range from 0.4 to 0.6 V,[28] suggesting the ORR reactions proceed mainly with an $n = 4e^-$ reaction pathway.[17] The stability of WAD-900 (Fig. 7d) was tested in a 0.1 M KOH solution saturated with O_2, and the stability over 20 000 s was 95.9%, larger than the 82.6% of Pt/C, indicating that its stability is excellent and shows that under the same test conditions, WAD-900 has better long-term performance than Pt/C, which may be due to the strong covalent bond between C and P and the absence of metal agglomeration and migration.[7]

4. Conclusions

In this paper, wild *Angelica dahurica* was directly used for phosphorus-doped biomass carbon materials for the oxygen reduction reaction (ORR), where the content of P in WAD ranges from 1 to 2 at%. WAD-900 shows a high P–C content and a better half-peak potential, which is 30 mV lower than the half-peak potential of a commercial Pt/C (20%) catalyst, and the limiting current density is 4.54 mA cm^{-2}, which exceeds that of

commercial Pt/C (20%). The limiting current density shows the excellent reaction potential of carbon materials in many previous P-doped materials. The average number of transferred electrons of WAD-900 is close to four electrons. After 20 000 seconds of testing, WAD-900 maintains a good stability of 95.9%. The biological approach to P-doped materials derived from phosphorus-containing plants, which has shown excellent performance in oxygen reduction, is simple and controllable and provides a new idea for subsequent carbon doping based on the combination of iron and phosphorus.

Data availability

We declare that all the experimental data in this paper are obtained through experimental tests and have absolute authenticity. All relevant data are within the paper. The data can be shared after the article is published.

Conflicts of interest

There is no conflict of interest to declare.

Acknowledgements

This work was supported by the Zhanjiang Science and Technology Bureau (2019A03009, 2021A05230), Natural Science Foundation of Lingnan Normal University (QL1406, ZL1004), Guangdong Basic and Applied Basic Research Foundation (2023A1515011796, 2024A1515011908), and Research Foundation for Advanced Talents of Lingnan Normal University (ZL2021020).

References

1 M. Kim, K. L. Firestein, J. F. Fernando, X. Xu, H. Lim, D. V. Golberg, J. Na, J. Kim, H. Nara, J. Tang and Y. Yamauchi, Strategic design of Fe and N co-doped hierarchically porous carbon as superior ORR catalyst: from the perspective of nanoarchitectonics, *Chem. Sci.*, 2022, **13**(36), 10836–10845.

2 M. Kim, J. F. Fernando, Z. Li, A. Alowasheeir, A. Ashok, R. J. Xin, D. Martin, A. K. Nanjundan, D. V. Golberg, Y. Yamauchi and N. Amiralian, Ultra-stable sodium ion storage of biomass porous carbon derived from sugarcane, *Chem. Eng. J.*, 2022, **445**, 136344.

3 M. Kim, R. J. Xin, J. Earnshaw, J. Tang, J. P. Hill, A. Ashok, A. K. Nanjundan, J. Kim, C. Young, Y. Sugahara and J. Na, MOF-derived nanoporous carbons with diverse tunable nanoarchitectures, *Nat. Protoc.*, 2022, **17**(12), 2990–3027.

4 J. Wu, Z. Yang, X. Li, Q. Sun, C. Jin, P. Strasser and R. Yang, Phosphorus-doped porous carbons as efficient electrocatalysts for oxygen reduction, *J. Mater. Chem. A*, 2013, **1**, 9889–9896.

5 Z. W. Liu, F. Peng, H. J. Wang, H. Yu, W. X. Zheng and J. Yang, Phosphorus-doped graphite layers with high electrocatalytic activity for the O_2 reduction in an alkaline medium, *Angew. Chem., Int. Ed.*, 2011, **50**, 3257–3261.

6 J. Wu, C. Jin, Z. Yang and R. Yang, Synthesis of phosphorus-doped carbon hollow spheres as efficient metal-free electrocatalysts for oxygen reduction, *Carbon*, 2015, **82**, 562–571.

7 J. Wu, Z. Yang, Q. Sun, X. Li, P. Strasser and R. Yang, Synthesis and electrocatalytic activity of phosphorus-doped carbon xerogel for oxygen reduction, *Electrochim. Acta*, 2014, **127**, 53–60.

8 C. Zhang, N. Mahmood, H. Yin, F. Liu and Y. Hou, Synthesis of phosphorus-doped graphene and its multifunctional applications for oxygen reduction reaction and lithium ion batteries, *Adv. Mater.*, 2013, **25**, 4932–4937.

9 W. Lei, Y. P. Deng, G. Li, Z. P. Cano, X. Wang, D. Luo and Z. Chen, Two-dimensional phosphorus-doped carbon nanosheets with tunable porosity for oxygen reactions in zinc-air batteries, *ACS Catal.*, 2018, **8**, 2464–2472.

10 R. Li, Z. Wei, X. Gou and W. Xu, Phosphorus-doped graphene nanosheets as efficient metal-free oxygen reduction electrocatalysts, *RSC Adv.*, 2013, **3**, 9978–9984.

11 X. Gong, S. Liu, C. Ouyang, P. Strasser and R. Yang, Nitrogen- and phosphorus-doped biocarbon with enhanced electrocatalytic activity for oxygen reduction, *ACS Catal.*, 2015, **5**, 920–927.

12 R. Li, F. Y. Zheng, X. Zhang, J. Hu, C. Xu and Y. Zhang, Phosphorus and iron doped nitrogen-containing carbon derived from biomass for oxygen reduction under various pH conditions, *Int. J. Hydrogen Energy*, 2020, **45**, 28651–28663.

13 X. Wei, X. Luo, H. Wang, W. Gu, W. Cai, Y. Lin and C. Zhu, Highly-Defective Fe-N-C Catalysts towards pH-Universal Oxygen Reduction Reaction, *Appl. Catal., B*, 2019, **263**, 118347.

14 X. Rao, Y. Lou, J. Chen, H. Lu, B. Cheng, W. Wang and S. Zhong, Polyacrylonitrile hard carbon as anode of high rate capability for lithium ion batteries, *Front. Energy Res.*, 2020, **8**, 3.

15 C. Zamora-Ledezma, L. Añez, J. Primera, P. Silva, S. Etienne-Calas and E. Anglaret, Photoluminescent single wall carbon nanotube-silica composite gels, *Carbon*, 2008, **46**, 1253–1255.

16 X. Qiao, H. Peng, C. You, F. Liu, R. Zheng, D. Xu and S. Liao, Nitrogen, phosphorus and iron doped carbon nanospheres with high surface area and hierarchical porous structure for oxygen reduction, *J. Power Sources*, 2015, **288**, 253–260.

17 H. Jiang, Y. Zhu, Q. Feng, Y. Su, X. Yang and C. Li, Nitrogen and phosphorus dual-doped hierarchical porous carbon foams as efficient metal-free electrocatalysts for oxygen reduction reactions, *Chem.–Eur. J.*, 2014, **20**, 3106–3112.

18 C. H. Choi, M. W. Chung, S. H. Park and S. I. Woo, Additional doping of phosphorus and/or sulfur into nitrogen-doped carbon for efficient oxygen reduction reaction in acidic media, *Phys. Chem. Chem. Phys.*, 2013, **15**, 1802–1805.

19 K. Kamiya, K. Hashimoto and S. Nakanishi, Instantaneous one-pot synthesis of Fe-N-modified graphene as an efficient electrocatalyst for the oxygen reduction reaction in acidic solutions, *Chem. Commun.*, 2012, **48**, 10213–10215.

20 F. Y. Zheng, R. Li, S. Ge, W. R. Xu and Y. Zhang, Nitrogen and phosphorus co-doped carbon networks derived from shrimp shells as an efficient oxygen reduction catalyst for microbial fuel cells, *J. Power Sources*, 2020, **446**, 227356.
21 A. K. Geim and K. S. Novoselov, The rise of graphene, *Nat. Mater.*, 2007, **6**, 183–191.
22 H. Wang, T. Maiyalagan and X. Wang, Review on recent progress in nitrogen-doped graphene: synthesis, characterization, and its potential applications, *ACS Catal.*, 2012, **2**, 781–794.
23 C. H. Choi, S. H. Park and S. I. Woo, Binary and ternary doping of nitrogen, boron, and phosphorus into carbon for enhancing electrochemical oxygen reduction activity, *ACS Nano*, 2012, **6**, 7084–7091.
24 H. J. Yan, B. Xu, S. Q. Shi and C. Y. Ouyang, First-principles study of the oxygen adsorption and dissociation on graphene and nitrogen doped graphene for Li-air batteries, *J. Appl. Phys.*, 2012, **112**, 104316.
25 X. Qiao, S. Liao, C. You and R. Chen, Phosphorus and nitrogen dual doped and simultaneously reduced graphene oxide with high surface area as efficient metal-free electrocatalyst for oxygen reduction, *Catalysts*, 2015, **5**, 981–991.
26 X. Mao, Z. Cao, Y. Yin, Z. Wang, H. Dong and S. Yang, Direct synthesis of nitrogen and phosphorus co-doped hierarchical porous carbon networks with biological materials as efficient electrocatalysts for oxygen reduction reaction, *Int. J. Hydrogen Energy*, 2018, **43**, 10341–10350.
27 L. Zheng, Y. Dong, B. Chi, Z. Cui, Y. Deng, X. Shi and S. Liao, UIO-66-NH_2-Derived Mesoporous Carbon Catalyst Co-Doped with Fe/N/S as Highly Efficient Cathode Catalyst for PEMFCs, *Small*, 2019, **15**, 1803520.
28 L. Zhao, Natural phosphorus-doped honeycomb carbon materials as oxygen reduction catalysts derived from Pulsatilla chinensis (Bunge) Regel, *RSC Adv.*, 2017, **7**, 13904–13910.